International Journal of Advanced Technology in Engineering and Science
Vol. No. 10, Issue No. 06, June 2022
www.ijates.com
ijates
ISSN 2348 - 7550

NUMERICAL SIMULATION FOR CBTS THIN FILM SOLAR CELLS – USING SCAPS – 1D

Dr. M. Suresh Kumar[1], CVS Harsha Vardhan[2], Vemana Siva Kumar[3], Chammampati Kesava Balramkumar[4], Dharmavaram Thulasi Teja[5], Degasikshu Ligeswar[6]

[1]Assosiate Professor, Dept. of ECE, S V College of Engineering, Tirupati, A.P, India.

[23456]B.Tech Students, Dept. of ECE, S V College of Engineering, Tirupati, A.P, India.

ABSTRACT

Cu_2BaSnS_4 (CBTS)-based solar cells show a promising performance in the field of sunlight-based energy production system. To increase the performance of CBTS-based solar cell, buffer layer optimization is still an obstacle. In this work, numerical simulations were performed on structures based on CBTS absorber layer, i-ZnO window layer, and transparent conducting layer n-ITO with different buffer layers using SCAPS-1D software to find a suitable buffer layer. Cadmium sulfide (CdS), zinc sulfide (ZnS) and their alloy cadmium zinc sulfide ($Cd_{0.4}Zn_{0.6}S$) ,Tin Sulfide(SnS_2), Molybdenum sulfide(MoS_2) were used as potential buffer layers to investigate the effect of buffer thickness, absorber thickness and temperature on open-circuit voltage (V_{oc}), short-circuit current (J_{sc}), fill factor (FF) and efficiency (η) of the solar cell. The optimum efficiencies using these three buffer layers are around 9.28%. Among these three buffers, $Cd_{0.4}Zn_{0.6}S$ is more preferable as CdS suffers from toxicity problem and ZnS shows drastic change in performance parameters. The simulation results can give important guideline for the fabrication of high-efficiency CBTS solar cell.

INTRODUCTION

Global energy consumption has increased dramatically with the growth of the world population and the development of industrialization. In the present circumstances, the amount of energy that is generated to meet the current demands for sustainable development of civilization is still inadequate. It is estimated that the world's energy consumption will increase by almost 50% by 2040. Today, nearly 80% of the global power generation emanates from nuclear and fossil fuels. Since the 1850s, when we began commercial drilling of oil from the depths of the earth's crust, we still rely heavily on driving our cars with liquid petroleum (gasoline). So far, the main source of electricity is generated from fossil fuels such as coal, oil and natural gas. However, these conventional energy sources face multiple challenges including rising prices, global warming and security concerns on imports from a restricted number of countries that have considerable fossil fuel supplies. The combustion of fossil fuels is one of the primary causes of global warming. Coal contains 78 % of carbon, which is the main contributor to global warming. Also, the by product "coal ash" produced during the combustion process can cause radiation and many other environmental dangers. The electricity produced through the use of

natural gas could not meet the world's growing demand. Also, natural gas produces toxic by-products, which questions the environmental safety. The result of these challenges triggered in search for an alternative source of energy and new technologies for electricity generation. The non-conventional and renewable energy sources such as solar, biomass, geothermal, hydroelectric and wind power generation are emerging as potential alternatives that address some of these concerns.

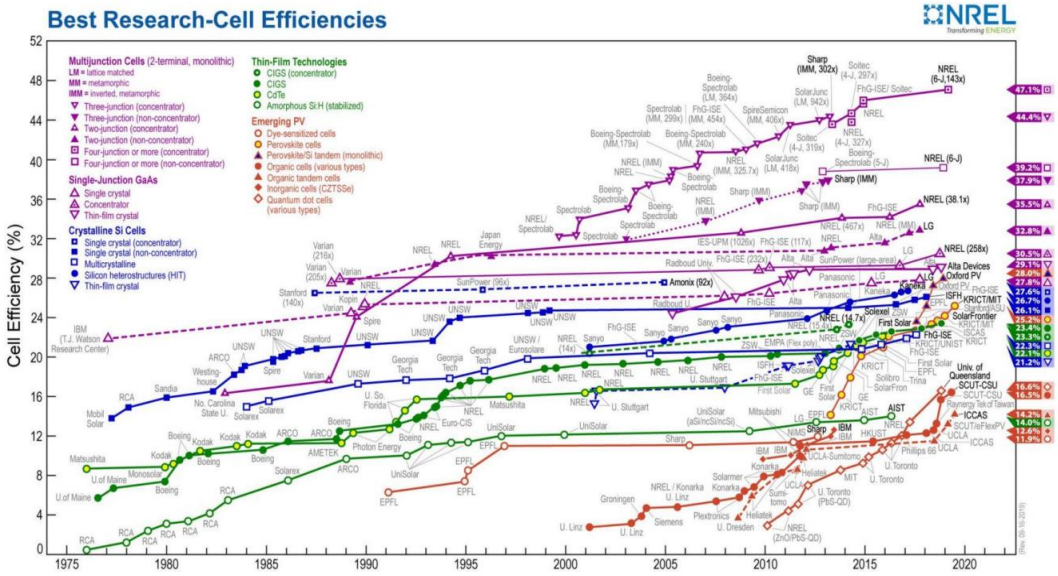

Fig 1: A chart of Conversion efficiencies of best research solar cells worldwide for various photovoltaic technologies since 1976 maintained by the USA National Renewable Energy Laboratory [1].

Why Solar Energy is important?

Solar energy is a major renewable energy source which is seen as a potential alternative that tends to some of these concerns with respect to its sustainability. Solar energy is a vast, inexhaustible, cheap, safe and versatile renewable power source that is harness able almost all over the world. Recent trends propose that solar energy will play an important role in energy production in the future. In fact, solar energy has the ability to fulfill all global energy needs. The sun emits on average nearly 120,000 TW of electromagnetic radiation on the surface of the Earth, which far exceeds the real needs of the human being. In particular, most part of the places in India receives about 4-7 kWh per sq. m per day of energy from the sun. For high populated countries like India, this vast amount of solar energy is appealing to be an attractive source of electricity. Photovoltaic (PV) technology, directly converts inexhaustible solar energy to clean electricity.

Generations of solar cells

Based on the different materials and technologies, the solar cells are usually categorized into four main generations up to recent years. The updated conversion efficiencies of the best research solar cells for various photovoltaic technologies published by USA National Renewable Energy Laboratory (NREL) are shown in Fig. 1

First Generation (1G) Solar cells

First-generation solar cells are the most dominant and matured in terms of fabrication processes and technology that are relatively expensive to produce. Traditionally, they are made of either crystalline silicon (c-Si) or GaAs wafers by the diffusion process. Silicon wafer-based solar cells continue to dominate the commercial production of solar cells and account for more than 86% of the terrestrial solar cell market. The highest commercial module efficiency for monocrystalline and polycrystalline silicon solar cells is 21.5% and 16.2% respectively. The monocrystalline silicon solar cells are made from one crystal with no defects accounting for better efficiency compared to polycrystalline solar cells having more defects. But the solar cells produced from the polycrystalline wafer are easier and cheaper which makes it competitive with monocrystals.

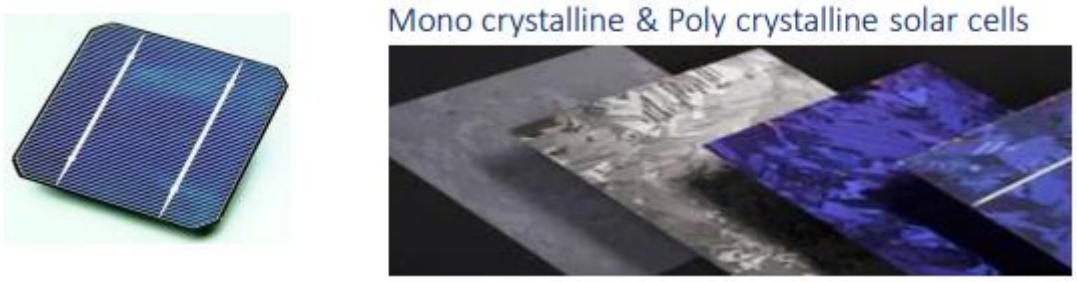

Fig.2 First Generation Solar cells

Second Generation (2G) Solar cells

Second-generation solar cells are generally termed as thin-film solar cells or thin-film photovoltaic cells and are made by depositing layers of semiconductor materials on a substrate only a few nanometers to tens of micrometers thick. The utilization of fewer materials and lower cost manufacturing processes allows to produce cheaper solar cells than first-generation solar cells but have lower efficiencies. Cadmium telluride (CdTe), copper indium gallium selenide (CIGS) and amorphous silicon are some of the most successful second generation materials which are commercially available in the market. The main advantage of these thin-film solar cells is that they do not have fingers in front for metallization and hence they are much applicable for applications on windows, cars, etc. In addition, these thin films can be grown on flexible substrates and are advantageous for producing large-area cells up to 6 m^2 . The thin film such as $Cu(In,Ga)Se_2$ (CIGS) and CdTe have demonstrated a high power conversion efficiency (PCE) of 22.6% [2] and 22.1% [3] respectively.

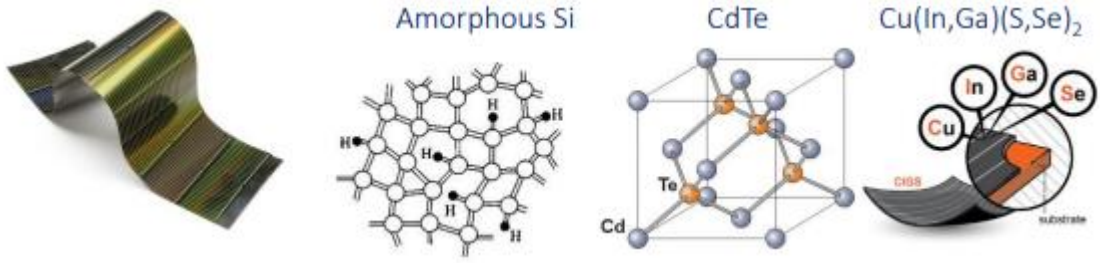

Fig.3 Second Generation Solar cells

Third Generation (3G) Solar cells

The fundamental purpose of this technology is to improve commercially available solar cells by making them efficient over the wider band of solar energy using various types of materials and techniques. The third-generation solar cells include concentrated solar cells, Dye-sensitized solar cells, Polymer-based solar cells, and Nanocrystal based solar cells. These are the novel and promising technologies and are not yet proven. The efficiency of the concentrated solar cells is higher and the total cost is lower than the conventional systems. The main principle of this technology is to concentrate a large amount of solar radiation on to a smaller region of the solar cell.

Fig.4 Third Generation Solar cells

Fourth Generation (4G) Solar cells

This hypothetical generation of solar cells includes hybrid solar cells that combine the low cost/flexibility of conducting polymer with the stability of novel inorganic nanostructures. This improves the power conversion efficiency and more efficient and cheaper solar cells than the current 3G solar cells. It is strongly believed that 4G solar cells would be a promising technology for the near future.

Why thin-film solar cells?

Thin-film solar cells belong to the 2G PV technology, in which the active material used as an absorber layer is usually few μm thick and has an absorption coefficient 100 times higher than that of Crystalline Si (c-Si) technology. The main bottleneck in terrestrial c-Si solar cells is its efficiency and cost, which undermines its acceptability in the domestic and industrial sectors. In 1G PV devices, approximately 50% of the total module cost is due to the cost of the wafer. The interesting asset of thin-film technology is that the main cost component of c-Si solar devices can be replaced and produced in flexible and lightweight substrates such as polyamide and various metal foils. In addition, the minimal use of the high purity materials in the production of the thin film PV devices allows a great decline in the device cost. Thus the energy payback time of the thin-film PV technology is low compared to the c-Si PV technology. Also based on our requirements, by varying the composition, the bandgap of the thin film materials can be tuned toutilize the wide range of solar spectrum and higher efficiency can be achieved fulfilling the increased energy requirements. Over the past few decades, chalcogenide-based thin-film solar cells such as $Cu(In,Ga)(S,Se)_2$ (CIGS) and CdTe have shown substantial improvement in the device efficiency and now reached the level of mass production. Recently, solar cells including CIGS and CdTe exhibit efficiencies very near to first-generation photovoltaic technology and use reduced materials thereby reducing associated costs. Among the different types of solar cells, the CIGS based

thin-film solar cells have received great attention due to their good stability and high power conversion efficiency (PCE).

Methodology and device structure

SCAPS-1D, one-dimensional solar cell simulation software developed at the Department of Electronics and Information Systems (EIS), University of Gent, Belgium, was used for numerically analysing the solar cell. Up to seven different layers can be added in the cell definition panel of the software which makes it more suitable for solar cell simulation. Physical properties such as bandgap, electron affnity, dielectric permittivity, etc., for different layers can be modified in the layer properties panel which helps to achieve the desired structure. The necessary working point specification can be indicated in the action panel. The software supports grading of all physical parameters and also specifcation of properties of front and back contact. A large number of AC and DC electrical measurements including short-circuit current density (J_{sc}), fll factor (FF), open-circuit voltage (V_{oc}), conversion effciency (η), quantum effciency (QE), spectral response, generation and recombination profile can be calculated as well as displayed using the software SCAPS-1D, compared to other simulation software [18].

Figure 5 shows the solar cell structure used in this study. The structure started with soda lime glass substrate. A thin MoS_2 layer of thickness of 100 nm to avoid high series resistance was used over the absorber layer, as this layer can be experimentally formed by the reaction of Mo back contact with sulfur contained in the absorber precursor (ZnS or SnS) in the case of CBTS solar cell [19]. The next layer was CBTS absorber layer in which most of the incident photons were absorbed to produce electron–hole pairs. CdS or ZnS or Cd0.4Zn0.6S or Mos_2 or SnS_2 buffer layer was used after that to provide the band alignment between CBTS and following window layer. Afterwards, less costly and available intrinsic zinc oxide (i-ZnO) of thickness of 80 nm was used for the window layer over the buffer layer which enhances light scattering to enable the efficient use of sun light to maximize the number of incident photons to the buffer and absorber layers [20]. Finally, a transparent conducting film n-type indium tin oxide (n-ITO) of thickness of 60 nm was used to provide a high mobility leading to an increase in visible absorption to obtain a lower sheet resistance [21].

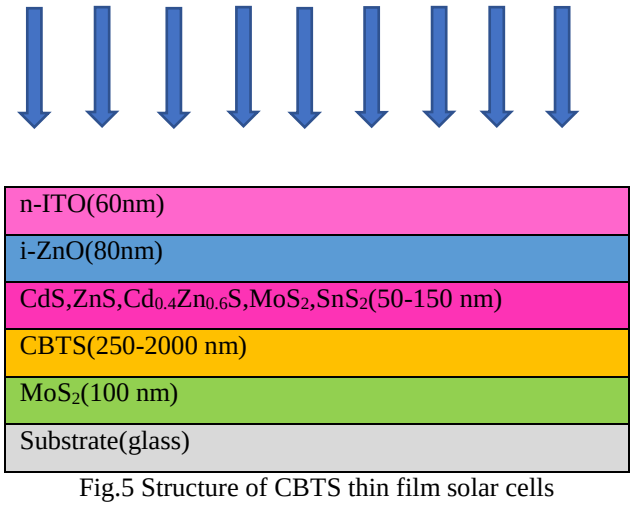

Fig.5 Structure of CBTS thin film solar cells

The illumination of light was through the side of n-ITO layer with "Air mass 1.5 global" spectrum with 1000 W/ m2 light power at 25 °C. In this work, the effect of series or shunt resistance was not considered. Two types of single layer defect were introduced in the absorber layer and buffer layer for the simulations. The values of the physical parameters used in this study are all taken from experimental study, different literatures or reasonable estimates [15, 22–25] which are summarized in Table 1. The observation of CBTS solar cell performances was performed in three different steps. In the first step, the buffer layer's thickness was varied from 50 to 150 nm with equal steps of 25 nm while keeping the absorber layer fixed at 2000 nm. The optimum thickness of the buffer layer was determined and then using it, the performance parameters were calculated and presented for each structure. In the next step, the buffer layer was fixed at its optimum thickness and the CBTS absorber layer was varied for the range of 250–2000 nm with a step size of 250 nm. Then, using the obtained CBTS optimum thickness for their respective buffer layer, the performance parameters were simulated and displayed in this case. Finally, the effect of temperature was observed for each structure by varying the temperature from 290 to 350 K with equal steps of 10 K. It is to be mentioned that for each step the other layers thickness and the material properties were fixed at their respective values.

Table.1 Physical parameters of different layers

Parameters	**CBTS**	**CdS**	**ZnS**	**MoS_2**	**SnS_2**	**$Cd_{0.4}Zn_{0.6}S$**
Thickness(nm)	2000	50-150	50-150	50-150	50-150	50-150
Bandgap(eV)	1.9	2.45	3.5	1.7	2.24	2.98
Electron affinity(eV)	3.6	4.4	4.5	4.2	4.24	4.2
Dielectric permittivity	5.4	9	10	13.60	10	9.4
CB effective density of states(cm^{-3})	2.2E+18	1.8E+19	1.8E+19	2.2E+18	2.2E+18	2.2E+18
VB effective density of states(cm^{-3})	1.8E+19	2.4E+18	1.8E+18	1.8E+19	1.8E+19	1.8E+19
Electron thermal velocity(cm s^{-1})	1.0E+7	1.0E+7	1.0E+7	1.0E+7	1.0E+7	1.0E+7
Hole thermal velocity(cm^{-1})	1.0E+7	1.0E+7	1.0E+7	1.0E+7	1.0E+7	1.0E+7
Electron mobility(cm^2/v_s)	30	100	100	100	5E+2	2.7E+2
Hole mobility(cm^2/v_s)	10	25	25	25	5E+1	2.7E+1
Shallow uniform donor density,N_D(cm^{-3})	0	5E+18	5E+15	1E+16	1E+17	1E+17
Shallow uniform acceptor density,N_A(cm^{-3})	1E+15	0	10	0	0	0
Defect type	Donor	Acceptor	Acceptor	Acceptor	Acceptor	Acceptor

Defect density(cm^{-3})	1E+15	1E+15	1E+15	1E+15	1E+15	1E+15

RESULTS AND DISCUSSION

Effect of buffer layer's thickness

To investigate the effect of buffer layer's thickness, simulations were done on the structure shown in Fig. 1 with different buffer layers. As already mentioned in Sect. 2, the buffer layer thickness was varied from 50 to 150 nm with a fixed CBTS layer of 2000 nm for the first steps of simulation. A single acceptor-type defect with defect density of $1 \times 10^{15} cm^{-3}$ was introduced in the buffer layer [25]. Figure 2 shows the variation of solar cell parameters such as open-circuit voltage (V_{oc}), short-circuit current density (J_{sc}), fill factor (FF) and efficiency (η) with the increase in buffer layer thickness. In Fig. 2 (for all graphs), the black line shows the variations for CdS, the red line for ZnS and the blue line for SnS_2 and the pink line for MoS_2 and the green line for $Cd_{0.4}Zn_{0.6}S$ buffer. In Fig. 2a, the V_{oc} vs. buffer layer thickness is shown where an increasing trend is found for MoS_2 from 60nm and decreasing trend is found for ZnS from 60nm whereas for CdS, ZnS and $Cd_{0.4}Zn_{0.6}S$, buffer layer change is too small to be found. ZnS buffer layer has higher bandgap with respect to the other four buffer layer. Next, the change in J_{sc} is shown where rapid decrease in J_{sc} is observed for MoS_2 buffer layer and moderate decrease in J_{sc} is observed for SnS_2 and CdS and very slight decrease is observed in $Cd_{0.4}Zn_{0.6}S$ and ZnS buffer layers. MoS_2 buffer layer possesses lower value of J_{sc} than the four other buffer layers. The decrease in short-circuit density results due to the less production of electron–hole pair as less number of electron–hole pair can reach the absorber layer with increase in buffer layer thickness. . In the case of fill factor, the decreasing behaviour for ZnS can be seen around 65 nm in Fig. 2c whereas the fill factor for CdS, SnS_2, and $Cd_{0.4}Zn_{0.6}S$ do not show any change and MoS_2 shows light increase in fill factor. The fill factor of ZnS decreases from 65 nm hereafter due to the effect of series resistance which increase with thickness and reduces the maximum achievable power output [27]. Finally, Fig. 2d shows the efficiency curves for the different buffer layers. The efficiency of the solar cell for ZnS buffer layers falls to almost 3.19% at 150 nm thickness whereas for CdS, SnS_2 and MoS_2 buffers the efficiencies decrease slightly and almost constant incase of $Cd_{0.4}Zn_{0.6}S$. The efficiencies are changed due to the combined effect of V_{oc}, J_{sc} and fill factor. Note that the solar cell performance can also decrease due to the additional trapping layers created by the defect, which can trap the incident photon [28]. The obtained optimum efficiencies for CdS, ZnS, SnS_2,MoS_2 and $Cd_{0.4}Zn_{0.6}S$ buffers are 6.74%, 3.91%, 7.41%, 4.31%, 8.85%.

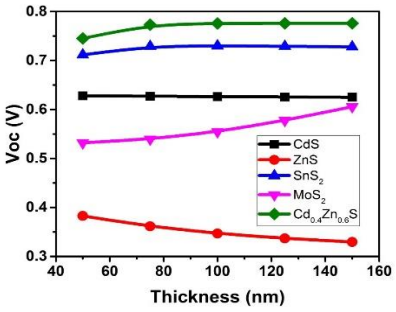

(a)

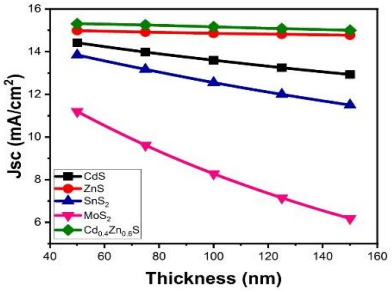

(b)

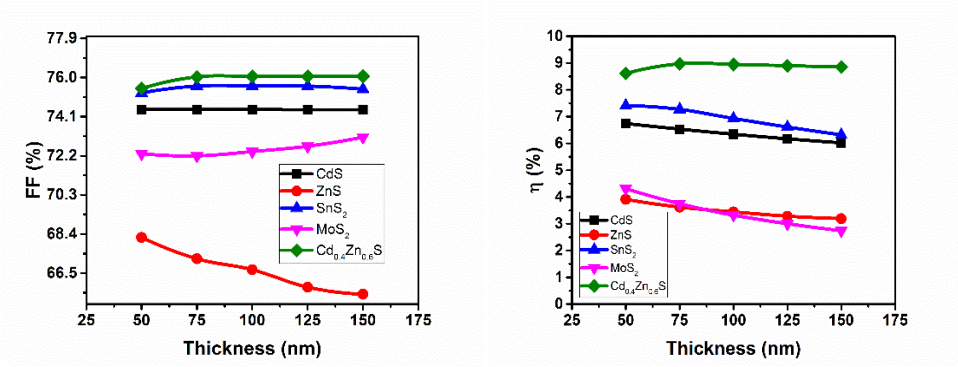

(c) (d)

Fig 6. **a** V_{oc} vs. buffer layer thickness. **b** J_{sc} vs. buffer layer thickness. **c** Fill Factor vs. buffer layer thickness. **d** Efficiency vs. buffer layer thickness.

Effect of CBTS absorber layer's thickness

The effect of CBTS thickness on solar cell performance was observed through simulations in three different structures CdS/CBTS, ZnS/CBTS, SnS_2/CBTS, MoS_2/CBTS and $Cd_{0.4}Zn_{0.6}S$/CBTS. For each simulation, the thickness of CBTS was varied from 250 to 2000 nm with a fixed buffer layer thickness of 75 nm at a temperature of 300 K. A single donor-type defect with a defect density of 1×10^{15} cm^{-3} was introduced in the CBTS layer.

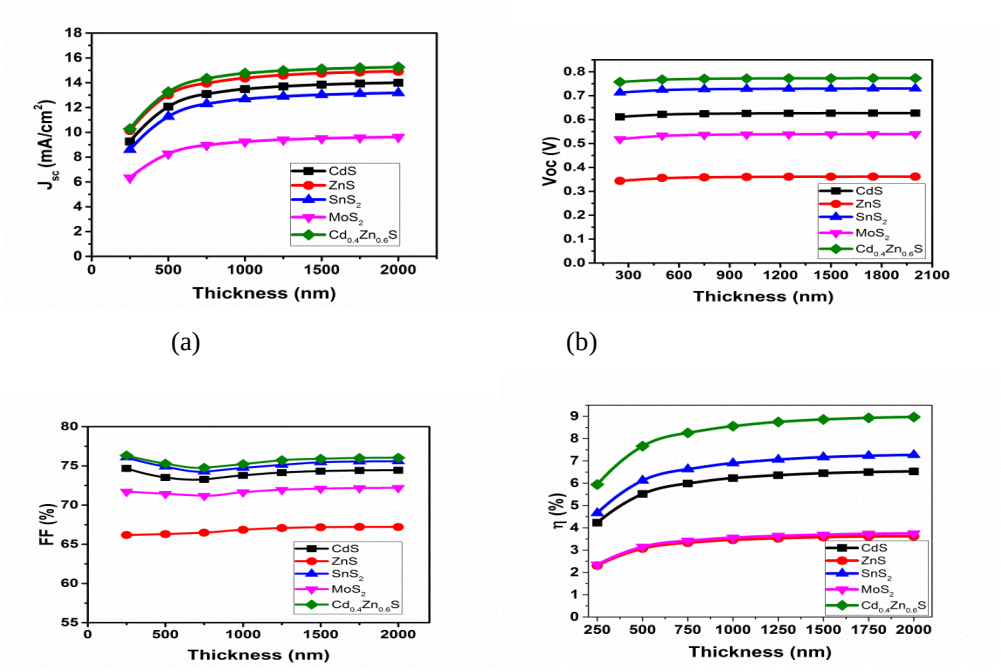

(a) (b)

(b) (d)

Fig. 7 **a** V_{oc} vs. absorber layer thickness. **b** J_{sc} vs. absorber layer thickness. **c** Fill factor vs. absorber layer thickness. **d** Efficiency vs. absorber layer thickness

Figure 7a–d shows the variation of open-circuit voltage (*V*oc), short-circuit current density (*J*sc), fill factor (FF) and efficiency (η), respectively, with increasing absorber layer's thickness. In each figure, the black curve shows the variation for CdS/CBTS structure, the red curve for ZnS/CBTS, the blue curve indicates the SnS2/ CBTS structure, the pink curve for MoS2/CBTS and the green curve for Cd0.4Zn0.6S/ CBTS. It is evident from Fig. 7 that all the parameters such as *V*oc, *J*sc, FF and η are low at lower thickness of CBTS layer (nearly 250–550 nm) which results due to the high recombination of the photo-generated carriers which recombines before reaching the buffer layer/CBTS layer interface. All the parameters then start to increase with the increase in CBTS thickness because the thicker CBTS layer will absorb more photons and generates more electron–hole pairs. The best efficiencies for CdS/CBTS, ZnS/CBTS, SnS2/ CBTS, MoS2/CBTS and Cd0.4Zn0.6S/CBTS structures were found 6.53%,3.62%,7.27%,3.75%,8.97% at 2000nm.

Effect of working temperature

In this section, the effect of temperature was observed for each structure by varying it from 290K to 350K. For CdS/CBTS, ZnS/CBTS, SnS_2/CBTS, MoS_2/CBTS and $Cd_{0.4}Zn_{0.6}S$/CBTS structures, the CBTS absorber layer's thickness was kept fixed at 2000 nm, respectively, while the buffer layer's thickness was fixed at 75 nm for every structure. The alteration of open-circuit voltage (*V*oc), short-circuit current density(*J*sc), fill factor (FF) and efficiency (η) with increasing temperature is shown Fig.8 where the black, red, blue, pink and green lines represent the changes in CdS/CBTS, ZnS/CBTS, SnS_2/CBTS, MoS_2/CBTS and $Cd_{0.4}Zn_{0.6}S$/CBTS structures separately.

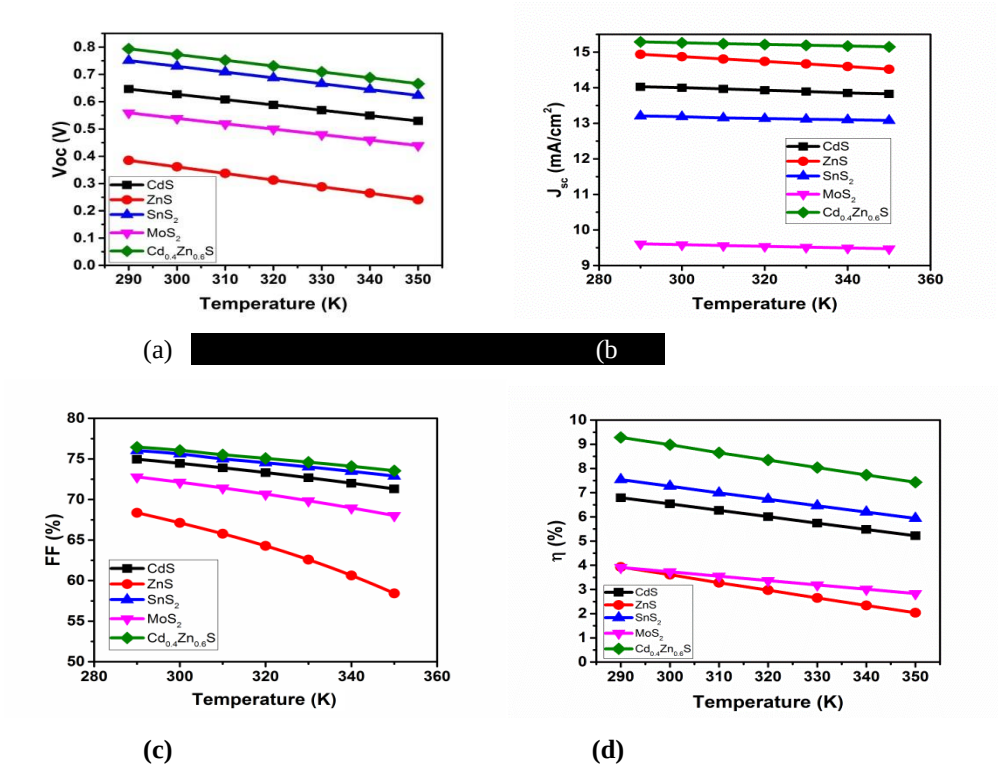

Fig. 8 **a** V_{oc} vs. temperature. **b** J_{sc} vs. temperature. **c** Fill factor vs. temperature. **d** Efficiency vs. temperature

When the temperature increases, there is an increase in the energy of electrons thus the bandgap of the material decreases. The electrons gaining extensive energy thus recombine with other holes. As a result, recombination rate of internal carrier increases resulting in decreasing V_{oc} and efficiency. This effect can be understood quite well from Fig. 8. In Fig. 8a, V_{oc} decreases almost linearly with increasing temperature. This is due to the reverse saturation current which increases with temperature and reduces the saturation current to decrease the open-circuit voltage. The change of J_{sc} is very small with increasing temperature shown in Fig. 8b as recombination process starts to dominate. Whereas the fill factor first increases with temperature as the resistance effect decreases. But it decreases for higher temperature due to light-induced degradation which can be seen from Fig. 8c. Finally, from Fig. 8d, the effect of increase in temperature on solar cell efficiency can be observed which shows a decreasing behaviour due to the combined effect of V_{oc}, J_{sc} and fill factor. From the simulation, the best efficiencies for CdS/CBTS, ZnS/CBTS, SnS_2/ CBTS, MoS_2/CBTS and $Cd_{0.4}Zn_{0.6}S$/CBTS were found 6.79%, 3.93%,7.54%,3.91% and 9.28% respectively, at a temperature of 290 K.

CONCLUSION

In this work, numerical simulations were performed for CBTS solar cell using five different buffer layers such as CdS/CBTS, ZnS/CBTS, SnS_2/CBTS, MoS_2/CBTS and $Cd_{0.4}Zn_{0.6}S$/CBTS and the performance parameters were observed by varying buffer layer thickness, absorber layer thickness and temperature. The buffer layer thickness for all these five types was found 75 nm to obtain high efficiency CBTS solar cell. Among them the $Cd_{0.4}Zn_{0.6}S$ buffer layer used in the CBTS solar cell exhibited higher efficiency(8.97%). In all cases performance parameters are affected significantly with the increased buffer layer. Because the loss of incident photons increases with increased buffer thickness which results in lower short circuit density leading to lower efficiency of the solar cell. The lower limit of thickness of CBTS absorber layer was obtained 250 nm to avoid the recombination of photogenerated carriers for all five buffer layers. In contrast the higher limit of thickness of CBTS absorber layer were found 2000 nm respectively for CdS/CBTS, ZnS/CBTS, SnS_2/ CBTS, MoS_2/CBTS and $Cd_{0.4}Zn_{0.6}S$/CBTS buffer layers to avoid the effect of minority carrier recombination. The best obtained efficiency (8.97%) was found for 2000 nm thick CBTS layer using $Cd_{0.4}Zn_{0.6}S$ buffer layer. The effect of temperature in CBTS solar cell was also important. In all cases (using different buffer layers) the efficiency decreased if we go beyond 290 K, as in higher temperature there is an enhancement of internal recombination of photogenerated carriers. The optimization of this study can lead to fabrication of high-efficiency CBTS solar cell.

REFERENCES

[1] P. Jackson, R. Wuerz, D. Hariskos, E. Lotter, W. Witte, M. Powalla, Effects of heavy alkali elements in Cu(In,Ga)Se2 solar cells with efficiencies up to 22.6%, Phys. Status Solidi Rapid Res. Lett. 10 (2016) 583–586, https://doi.org/10.1002/ pssr.201600199.

[2] W. Wang, M.T. Winkler, O. Gunawan, T. Gokmen, T.K. Todorov, Y. Zhu, D.B. Mitzi, Device characteristics of CZTSSe thin-film solar cells with 12.6% efficiency, Adv. Energy Mater. 4 (2014), 1301465, https://doi.org/10.1002/aenm.201301465.

[3] M. Suresh Kumar, S.P. Madhusudanan, S.C. Kanth, K. Mohanta, S.K. Batabyal, Solution phase fabrication of photoactive Cu2BaSnS4 thin films for solar energy harvesting, J. Solid State Electrochem. 24 (2020) 305–311, https://doi.org/ 10.1007/s10008-019-04418-y.

[4] S.P. Madhusudanan, M. Suresh Kumar, K. Yamini Yasoda, D. Santhanagopalan, S. K. Batabyal, Photo-enhanced supercapacitive behaviour of photoactive Cu2FeSnS4 (CFTS) nanoparticles, J. Mater. Sci. Mater. Electron. 4 (2019), https://doi.org/ 10.1007/s10854-019-02582-5.

[5] D. Shin, T. Zhu, X. Huang, O. Gunawan, V. Blum, D.B. Mitzi, Earth-abundant chalcogenide photovoltaic devices with over 5% efficiency based on a Cu2BaSn(S, Se)4 absorber, Adv. Mater. 29 (2017) 1–7, https://doi.org/10.1002/ adma.201606945.

[6] Z. Xiao, W. Meng, J.V. Li, Y. Yan, Distant-atom mutation for better earth-abundant light absorbers: a case study of Cu2BaSnSe4, ACS Energy Lett. 2 (2017) 29–35, https://doi.org/10.1021/acsenergylett.6b00577.

[7] M. Suresh Kumar, K. Mohanta, S.K. Batabyal, Solution processed Cu2CdSnS4 as a low-cost inorganic hole transport material for polymer solar cells, Sol. Energy Mater. Sol. Cells 161 (2017) 157–161, https://doi.org/10.1016/j. solmat.2016.11.028.

[8] M. Suresh Kumar, S.P. Madhusudanan, S.K. Batabyal, Substitution of Zn in Earth Abundant Cu2ZnSn(S,Se)4 based thin film solar cells – A status review, Sol. Energy Mater. Sol. Cells 185 (2018) 287–299, https://doi.org/10.1016/j. solmat.2018.05.003.

[9] D. Shin, E. Ngaboyamahina, Y. Zhou, J.T. Glass, D.B. Mitzi, Synthesis and characterization of an earth-abundant Cu2BaSn(S,Se)4 chalcogenide for photoelectrochemical cell application, J. Phys. Chem. Lett. 7 (2016) 4554–4561, https://doi.org/10.1021/acs.jpclett.6b02010.

[10] D. Shin, B. Saparov, T. Zhu, W.P. Huhn, V. Blum, D.B. Mitzi, BaCu2Sn(S,Se)4: Earth abundant chalcogenides for thin-film photovoltaics, Chem. Mater. 28 (2016) 4771–4780, https://doi.org/10.1021/acs.chemmater.6b01832.

[11] J. Ge, Y. Yu, Y. Yan, Earth-abundant orthorhombic BaCu2Sn(SexS1-x)4 (x ≈ 0.83) thin film for solar energy conversion, ACS Energy Lett. 1 (2016) 583–588, https:// doi.org/10.1021/acsenergylett.6b00324.

[12] Z. Chen, K. Sun, Z. Su, F. Liu, D. Tang, H. Xiao, L. Shi, L. Jiang, X. Hao, Y. Lai, Solution-processed trigonal Cu2BaSnS4 thin-film solar cells, ACS Appl. Energy Mater. 1 (2018) 3420–3427, https://doi.org/10.1021/acsaem.8b00514.

[13] C.L. McCarthy, R.L. Brutchey, Solution deposited Cu2BaSnS4-xSex from a thiol amine solvent mixture, Chem. Mater. 30 (2018) 304–308, https://doi.org/ 10.1021/acs.chemmater.7b03931.

[14] M. Suresh Kumar, S.P. Madhusudanan, A.R. Rajamani, M. Siaj, S.K. Batabyal, Barium substitution in kesterite Cu2ZnSnS4: Cu2Zn1–xBaxSnS4 quinary alloy thin films for efficient solar energy harvesting, Cryst. Growth Des. (2020), https://doi. org/10.1021/acs.cgd.0c00150 acs.cgd.0c00150.

[15] J. Ge, Y. Yan, Synthesis and characterization of photoelectrochemical and photovoltaic Cu2BaSnS4 thin films and solar cells, J. Mater. Chem. C 5 (2017) 6406–6419, https://doi.org/10.1039/C7TC01678F.